mathematics

MDPI

Article

Adaptive Super-Twisting Sliding Mode Control of Active Power Filter Using Interval Type-2-Fuzzy Neural Networks

Jiacheng Wang [1], Yunmei Fang [2] and Juntao Fei [1,*]

[1] College of Information Science and Engineering, Jiangsu Key Laboratory of Power Transmission and Distribution Equipment Technology, Hohai University, Changzhou 213022, China
[2] College of Mechanical and Electrical Engineering, Hohai University, Changzhou 213022, China
* Correspondence: jtfei@hhu.edu.cn

Abstract: Aiming at the unknown uncertainty of an active power filter system in practical operation, combining the advantages of self-feedback structure, interval type-2 fuzzy neural network, and super-twisting sliding mode, an adaptive super-twisting sliding mode control method of interval type-2 fuzzy neural network with self-feedback recursive structure (IT2FNN-SFR STSMC) is proposed in this paper. IT2FNN has an uncertain membership function, which can enhance the nonlinear ability and robustness of the network. The historical information will be stored and utilized by the self-feedback recursive structure (SFR) at runtime. Therefore, the novel IT2FNN-SFR is designed to improve the dynamic approximation effect of the neural network and reduce the dependence of the controller on the actual mathematical model. The adaptive rate of each weight of the neural network is designed by the Lyapunov method and gradient descent (GD) algorithm to ensure the convergence and stability of the system. Super-twisting sliding mode control (STSMC) has strong robustness, which can effectively reduce system chattering, and improve control accuracy and system performance. The gain of the integral term in the STSMC is set as a constant, and the other gain is changed adaptively whose adaptive rate is deduced through the stability proof of the neural network, which greatly reduces the difficulty of parameter adjustment. The harmonic suppression ability of the designed control strategy is verified by simulation experiments.

Keywords: active power filter (APF); interval type-2 fuzzy neural network (IT2FNN); STSMC; self-feedback recursive structure

MSC: 68T07; 93C40

Citation: Wang, J.; Fang, Y.; Fei, J. Adaptive Super-Twisting Sliding Mode Control of Active Power Filter Using Interval Type-2-Fuzzy Neural Networks. *Mathematics* **2023**, *11*, 2785. https://doi.org/10.3390/math11122785

Academic Editors: Adrian Olaru, Gabriel Frumusanu and Catalin Alexandru

Received: 13 May 2023
Revised: 16 June 2023
Accepted: 19 June 2023
Published: 20 June 2023

1. Introduction

Nowadays, as countries around the world increasingly favor new energy power generation to improve the energy structure, the power grid is facing increasingly complex nonlinear loads, which will generate a large number of harmonics, presenting significant challenges to maintain the safe and stable operation of the grid [1–3]. Therefore, addressing harmonics in the grid is of utmost importance. One common solution is harmonic compensation, which achieves the goal by simply installing a parallel or series compensation device on the load side. Active power filters (APF) have become the primary equipment for harmonic compensation due to the flexibility, excellent compensation capabilities, and superior controllability when compared to passive power filters (PPF) [4,5]. The traditional harmonic current compensation tracking control (HCCTC) cannot fully utilize the superior characteristics of APF. It is the research direction of many researchers to design the novel HCCTC with better performance by incorporating various intelligent control theories.

Sliding mode control (SMC) is a highly robust, discontinuous nonlinear control method that is commonly used to address uncertainties and disturbances within a system [6–8]. In order to ameliorate chattering in SMC, researchers have come up with different methods.

In some studies, scholars improved the reaching law of sliding mode to reduce chattering and improve the convergence of the controller [9,10]. In one study, a novel nonsingular terminal sliding mode control (NTSMC) is designed to weaken the chattering in [11]. Due to the convergence property of the fractional-order algorithm, it is applied in the design of the SMC to reduce the chattering around the sliding surface and to enhance the robustness of the controller [12,13]. In [13], a controller is designed to combine the advantages of the nonsingular terminal sliding mode control and fractional-order sliding mode control, which has fast convergence, flexible control, and is chatter-free. Adaptive sliding mode control (ASMC) is also an approach to handle the chattering problem [14]. Roy et al. [15,16] developed two novel ASMC strategies successively, one of which removes the assumption of prior bounded uncertainty, and the other can solve the problem of overestimation or underestimation, further improving the robustness of the controller and reducing the chattering. In [17], a high-order sliding mode control (HOSMC) is proposed, to minimize chattering by removing the limitations of input–output relative order. A novel adaptive HOSMC is developed to enhance the chattering suppression ability [18]. As one of the HOSMC, second-order sliding mode control can effectively solve the chattering problem in the control of underactuated mechanical systems [19]. The super-twisting sliding mode (STSMC) applies to systems (typically of any order) where the control is present in the first derivative of the sliding variable. At the same time, it can produce continuous control signals to weaken the chattering [20]. In the field of speed and altitude tracking control of air-breathing hypersonic vehicles, a new composite controller combining STSMC, high-order disturbance observer, and backstepping control is designed [21]. In one study, a model-free controller was designed, which is combining STSMC and iterative learning laws, to be applied in the unknown dynamics tray indexing systems [22]. However, it may be difficult to adjust the gain of STSMC manually, and the performance of STSMC cannot be fully utilized. In this paper, the gain parameter of the integral term is selected manually, and the other gain is adjusted adaptively to reduce the difficulty of parameter selection.

The performance of STSMC can be further improved if the dynamic equations of the system can be predicted in advance and feed-forward compensation can be performed. Neural networks are commonly utilized due to their strong approximation ability [23–26]. In [23], a novel PID controller based on the NN is developed to adjust the minimum bandwidth for different situations automatically. For the design of the virtual unmodeled dynamic compensator, three-layer NNs were used to estimate unknowns in [24]. A neural network controller is proposed to adjust the sliding mode gain adaptively to reduce chattering [25]. Li et al. utilized the RBFNNs to estimate the unknown function in nonlinear systems [26]. The combination of fuzzy logic rules and neural networks can reduce the number of nodes of neural networks and improve the ability to deal with nonlinearity and robustness [27–30]. However, due to the fact that the Type-1 fuzzy method uses accurate and clear membership functions, the overall performance of the system could not reduce or eliminate the uncertainties effectively caused by changes in the environment and other factors. In view of the above problems, some scholars extend the interval type-1 to interval type-2, which makes the membership function uncertain, to further improve the nonlinear ability and robustness of the network [31–33]. However, FNNs could be regarded as static mapping, which has the defect of poor ability to deal with dynamics. To overcome the disadvantage of the poor dynamic ability of NNs, some scholars put forward a recursive neural network (RNN) by combining feedback structure with the network [34–40]. A fully connected recurrent NN is designed to approximate the exact mathematical dynamics in a real-time scene, which has a better ability for dynamic response, function approximation ability, and convergence speed [35]. A self-organizing RNN with novel adaptive algorithms is adopted to improve the accuracy of model prediction.

Motivated by the above research, an adaptive super-twisting sliding mode control method of interval type-2 fuzzy neural network with self-feedback recursive structure (IT2FNN-SFR STSMC) is proposed to ensure that the compensation current in the APF system can track the desired current quickly and accurately in this paper. The advantages

of the IT2FNN and RNN are concentrated in the novel IT2FNN-SFR, resulting in its better dynamic approximation capacity. The adaptive laws of parameters in the proposed IT2FNN-SFR STSMC are derived by the Lyapunov method and GD algorithm, and the stability and convergence of the designed controller are also proved by the Lyapunov method. Moreover, the simulation experiments have been carried out to verify that the harmonic suppression capability is in line with international standards and has good steady-state response and dynamic performance. In summary, the major contributions of this article are described as:

(1) A new structure of IT2FNN, namely IT2FNN-SFR, has been proposed, which has the ability of strong robustness as IT2FNN and great dynamic response as RNN. The new NN is error-driven and online optimization, which means it is less dependent on accurate and detailed information about the system. The recursive structure in the NN will store and take advantage of the historical information to improve the accuracy of estimation and dynamic approximation effect;

(2) STSMC not only has the advantages of strong robustness and simple control principle of traditional SMC but also overcomes the chattering problem. In order to reduce the inaccuracy and complexity of manual parameter setting, a sliding mode gain adaptive law is deduced to realize a set of gain optimal solutions.

The remainder of this article is structured as follows. In Section 2, the principle and ideal dynamic equation of a single-phase APF are presented. Section 3 details a novel control strategy and provides proof of its stability. Section 4 shows the simulation experiment to verify the effectiveness of the proposed method. Finally, Section 5 concludes this article.

2. Principle of Active Power Filter

Due to the high reliability of compensation performance and flexible use, APF is widely used in power systems for harmonic suppression. The main circuit of a single APF consists of a PWM inverter circuit and a large capacitor on the DC side for energy storage. The current and voltage signals of the power grid circuit are collected for harmonic analysis and compensation through the sensors. The pulse width modulation (PWM) signal is generated by processing these signals by the controller. Finally, the PWM inverter works out to generate the corresponding current for the system current.

Figure 1 depicts the typical block diagram of a single-phase APF system control, where u_s, U_{dc}, i_s, i_c, i_L are the supply voltage, the DC-link voltage, the grid current, the compensation current, and the load current of the APF circuit, respectively. L and R are the equivalent inductance and resistance of the APF circuit.

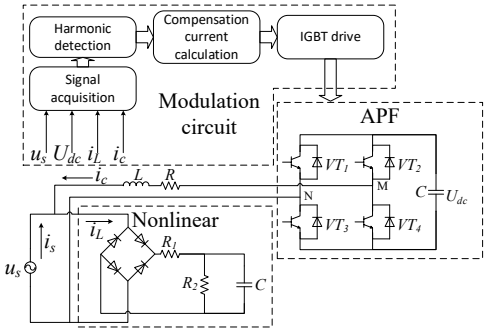

Figure 1. The block diagram of a single-phase active power filter.

According to Kirchhoff's voltage and current laws, the following equation can be obtained:

$$u_s = -L\frac{di_c}{dt} - Ri_c + U_{MN} \tag{1}$$

where U_{MN} is the output voltage of the DC side capacitor voltage modulated by the PWM inverter circuit.

Assuming that the control law of each cycle is $u \in [0,1]$, and the IGBTs are ideal, the working state is expressed as:

$$\begin{cases} VT_1, VT_4 \text{ is } on \text{ and } VT_2, VT_3 \text{ is } off. \ t \in [0,u] \\ VT_1, VT_4 \text{ is } off \text{ and } VT_2, VT_3 \text{ is } on. t \in [u,1] \end{cases} \tag{2}$$

Due to $U_{MN} \in [-U_{dc}, U_{dc}]$, the following relation can be obtained:

$$U_{MN} = (2u-1)U_{dc} \tag{3}$$

From (1) and (3), the ideal equation of compensation current is rewritten as:

$$\dot{i}_c = -\frac{R}{L}i_c - \frac{u_s}{L} - \frac{U_{dc}}{L} + \frac{2U_{dc}}{L}u \tag{4}$$

Hence, it can be abbreviated as:

$$\dot{x} = f_1(x) + bu \tag{5}$$

where x is the compensation current i_c.

$$f_1(x) = -\frac{R}{L}i_c - \frac{u_s}{L} - \frac{U_{dc}}{L} \tag{6}$$

$$b = \frac{2U_{dc}}{L} \tag{7}$$

Considering the internal parameters of the system often change uncertainly and the unknown external disturbances are existed in the system, the total disturbance containing parameter perturbation and external disturbances is defined as $g(t)$, assuming that it is bounded. The actual dynamic equation is given as:

$$\dot{x} = f + bu \tag{8}$$

where $f = f_1(x) + g(t) = -\frac{R}{L}i_c - \frac{u_s}{L} - \frac{U_{dc}}{L} + g(t)$.

3. Controller Design and Analysis

In order to improve the robustness of the system and reduce the chattering, the interval type-2-fuzzy neural networks with self-feedback recursive structure adaptive super-twisting sliding mode control (IT2FNN-SFR STSMC) strategy is designed. The block diagram is depicted in Figure 2. First, the structure of the novel networks is shown in Figure 3 and the basic functions and signal transmission of each layer are introduced as follows:

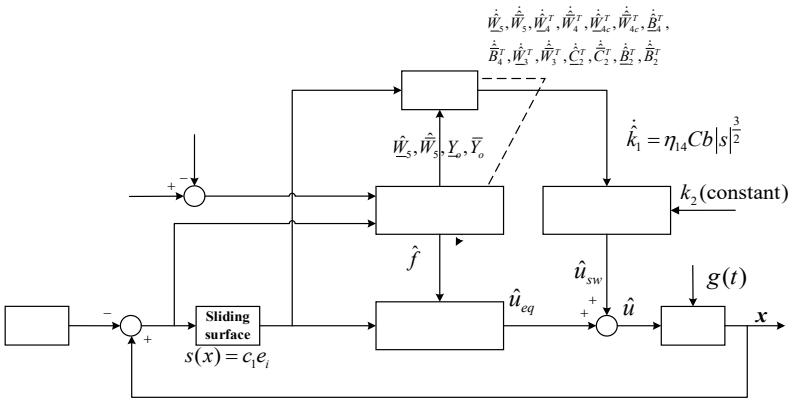

Figure 2. The block diagram of IT2FNN-SFR STSMC.

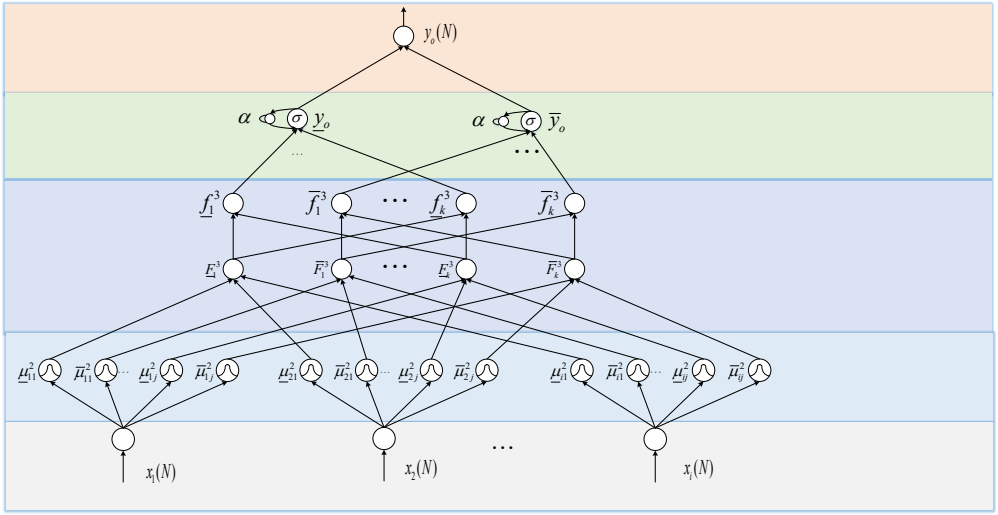

Figure 3. The structure of IT2FNN-SFR.

(1) Layer I (input layer): The input signals $X = \begin{bmatrix} x_1 & x_2 & \cdots & x_i \end{bmatrix}^T$ are transmitted in the layer, where the number of neurons in this layer is determined by the actual needs of the specific problem. In this paper, the current error and DC-side voltage error are used as the input of neural network, i.e., $i = 2$. The output of this layer is expressed as:

$$net_i^1(N) = x_i^1(N) \tag{9}$$

$$y_i^1(N) = f_i^1\left(net_i^1(N)\right) = net_i^1(N) \tag{10}$$

where $x_i^1(N)$ and $y_i^1(N)$ represent the input and output of the ith node in the first layer, respectively; N represents the number of sampling times.

(2) Layer II (membership function layer/fuzzy layer): In this layer, the Gaussian function with center vector and uncertain base width is selected to enhance the ability of neural network to deal with nonlinearity. Assume that the j-group type-2 fuzzy output set is $[\underline{\mu}_{ij}^2, \overline{\mu}_{ij}^2]$. In this paper, the number of output set is selected as 3, i.e., $j = 3$. The input–output transfer relation is expressed as:

$$x_{ij}^2(N) = y_i^1(N) \tag{11}$$

$$\underline{\mu}_{ij}^2(N) = \exp\left[-\frac{1}{2}\left(\frac{x_{ij}^2(N) - \underline{c}_{ij}^2}{\underline{\sigma}_{ij}^2}\right)^2\right] \tag{12}$$

$$\overline{\mu}_{ij}^2(N) = \exp\left[-\frac{1}{2}\left(\frac{x_{ij}^2(N) - \overline{c}_{ij}^2}{\overline{\sigma}_{ij}^2}\right)^2\right] \tag{13}$$

where μ_{ij}^2, c_{ij}^2, σ_{ij}^2 represent type-2 fuzzy output, center vector and base width of type 2 Gaussian fuzzy membership function, respectively; "$\underline{*}$", "$\overline{*}$" represent the lower and upper bounds of each variable, respectively.

(3) Layer III (Rule Layer): This layer integrates input signals from the Layer II. The number of neurons in the layer is the equal to the number of neurons in each group of the Layer II, i.e., $j = k = 3$. The signal transmission functions are expressed as:

$$\underline{F}_k^3 = \prod_{i=1}^{I} \underline{\mu}_{ij}^2 \tag{14}$$

$$\overline{F}_k^3 = \prod_{i=1}^{I} \overline{\mu}_{ij}^2 \tag{15}$$

$$\underline{f}_k^3 = \frac{\underline{F}_k^3}{\sum_{k=1}^{K} \underline{F}_k^3} \tag{16}$$

$$\overline{f}_k^3 = \frac{\overline{F}_k^3}{\sum_{k=1}^{K} \overline{F}_k^3} \tag{17}$$

where f_k^3 is the output of the rule layer after normalization.

(4) Layer IV (self-feedback recursive layer): This layer integrates the current and historical output information from the rule layer, and the temporary recursive layer is applied to reserve and process the history output information. In this layer, the group number of the layer is 1, i.e., $o = 1$. The output can be expressed as:

$$\underline{x}^4(N) = \sum \underline{\omega}_k^3 \underline{f}_k^3 \tag{18}$$

$$\underline{x}^{4c}(N) = \alpha \underline{x}^{4c}(N-1) + \underline{y}^4(N-1) \tag{19}$$

$$\underline{net}^4(N) = \underline{\omega}^4 \underline{x}^4(N) + \underline{\omega}^{4c} \underline{x}^{4c}(N) + \underline{b}^4 \tag{20}$$

$$\underline{y}^4(N) = \sigma\left(\underline{net}^4(N)\right) \tag{21}$$

$$\overline{x}^4(N) = \sum \overline{\omega}_k^3 \overline{f}_k^3 \tag{22}$$

$$\overline{x}^{4c}(N) = \alpha \overline{x}^{4c}(N-1) + \overline{y}^4(N-1) \tag{23}$$

$$\overline{net}^4(N) = \overline{\omega}^4 \overline{x}^4(N) + \overline{\omega}^{4c} \overline{x}^{4c}(N) + \overline{b}^4 \tag{24}$$

$$\overline{y}^4(N) = \sigma\left(\overline{net}^4(N)\right) \tag{25}$$

$$\sigma(z) = \frac{1}{1+e^{-z}} \tag{26}$$

where $x^4(N)$ represents the signal from the rule layer at the current sampling time; $x^{4c}(N)$ represents the historical information in the temporary recursive layer; ω^{4c} represents a self-feedback weight; ω^4 represents the weight of the SFR layer; α is the self-feedback parameter, which determines the proportion of historical information; b_l^4 is a bias term; $\sigma(\cdot)$ is a sigmod activation function.

(5) Layer V (output layer): the network is defuzzification through weighting. The expression is given as:

$$y_o(N) = \underline{\omega}^5 \underline{y}^4(N) + \overline{\omega}^5 \overline{y}^4(N) \tag{27}$$

Next, a new neural network is designed to estimate the actual model and reduce the dependence of the controller on the model. Meanwhile, super twisted sliding mode control (STSMC) is introduced to reduce the chattering. However, the traditional STSMC is complicated in adjusting parameters. In this paper, the adaptive rate of gain k_1 is also designed to reduce the difficulty of parameter adjustment when designing the adaptive rate of network parameters as shown in Figure 2.

Define the tracking error of APF system as:

$$e = x - r \tag{28}$$

where x is a tracking current, r is the reference current.

Design the sliding surface as:

$$s = Ce \tag{29}$$

where C is the gain of the sliding surface, which is the positive constant to be designed.

The derivative of Equation (29) is obtained as:

$$\dot{s} = C\left(\dot{x} - \dot{r}\right) = C\left(f + bu - \dot{r}\right) \tag{30}$$

The equivalent control law can be derived when $\dot{s} = 0$:

$$u_{eq} = \frac{1}{b}\left(-f + \dot{r}\right) \tag{31}$$

Adaptive STSMC is used to design the switching control law:

$$u_{sw} = -\hat{k}_1|s|^{\frac{1}{2}}\mathrm{sgn}(s) - \int k_2\mathrm{sgn}(s)dt \tag{32}$$

where $k_1 > 0$, $k_2 > 0$.

Substituting $\hat{f}$ into the control law, the control strategy can be established:

$$u = \frac{1}{b}(-\hat{f} + \dot{r}) - \hat{k}_1|s|^{\frac{1}{2}}\mathrm{sgn}(s) - \int k_2\mathrm{sgn}(s)dt \tag{33}$$

From the proposed neural network, the following results can be obtained:

$$\begin{aligned} f \quad &= \underline{W_5^*}^T\Phi^*(\underline{W_4^*}, \underline{W_{4c}^*}, \underline{B_4^*}, \underline{W_3^*}, \underline{B_2^*}, \underline{C_2^*}) \\ &+\overline{W_5^*}^T\Phi^*(\overline{W_4^*}, \overline{W_{4c}^*}, \overline{B_4^*}, \overline{W_3^*}, \overline{B_2^*}, \overline{C_2^*}) + \varepsilon \end{aligned} \tag{34}$$

where ε is the error between the optimal value and the actual value, and $\underline{C_2^*}$, $\overline{C_2^*}$, $\underline{B_2^*}$, $\overline{B_2^*}$, $\underline{W_3^*}$, $\overline{W_3^*}$, $\underline{W_4^*}$, $\overline{W_4^*}$, $\underline{W_{4c}^*}$, $\overline{W_{4c}^*}$, $\underline{W_5^*}$, $\overline{W_5^*}$, $\underline{B_4^*}$, $\overline{B_4^*}$ are the best parameters.

For the sake of further proof of brevity, define that:

$$\underline{\Phi} = \Phi(\underline{W_4}, \underline{W_{4c}}, \underline{B_4}, \underline{W_3}, \underline{B_2}, \underline{C_2}) \tag{35}$$

$$\overline{\Phi} = \Phi(\overline{W_4}, \overline{W_{4c}}, \overline{B_4}, \overline{W_3}, \overline{B_2}, \overline{C_2}) \tag{36}$$

The output of IT2FNN-SFR is used to replace the f, denoted as:

$$\hat{f} = y_o = \underline{\hat{W}_5}^T\underline{\hat{\Phi}} + \overline{\hat{W}_5}^T\overline{\hat{\Phi}} \tag{37}$$

where the superscript "$\wedge$" represent the estimated values of the corresponding parameters.

The estimation error of the designed neural network is:

$$\begin{aligned} \widetilde{f} \quad &= f - \hat{f} = \underline{W_5^*}^T\underline{\Phi^*} + \overline{W_5^*}^T\overline{\Phi}^* + \varepsilon - (\underline{\hat{W}_5}^T\underline{\hat{\Phi}} + \overline{\hat{W}_5}^T\overline{\hat{\Phi}}) \\ &= \underline{\hat{W}_5}^T\underline{\widetilde{\Phi}} + \underline{\widetilde{W}_5}^T\underline{\hat{\Phi}} + \overline{\hat{W}_5}^T\overline{\widetilde{\Phi}} + \overline{\widetilde{W}_5}^T\overline{\hat{\Phi}} + \varepsilon_0 \end{aligned} \tag{38}$$

where the superscript "$\sim$" represent the approximation errors; $\varepsilon_0 = \underline{\widetilde{W}_5}^T\underline{\widetilde{\Phi}} + \overline{\widetilde{W}_5}^T\overline{\widetilde{\Phi}} + \varepsilon$ is the total approximation error.

By expanding Taylor $\underline{\Phi}^*$ and $\overline{\Phi}^*$, respectively, we can get the following results:

$$\begin{aligned}\widetilde{\underline{\Phi}} &= \frac{\partial \underline{\Phi}}{\partial \underline{W}_4}\Big|_{\underline{W}_4=\hat{\underline{W}}_4}(\underline{W}_4^*-\hat{\underline{W}}_4)+\frac{\partial \underline{\Phi}}{\partial \underline{W}_{4c}}\Big|_{\underline{W}_{4c}=\hat{\underline{W}}_{4c}}(\underline{W}_{4c}^*-\hat{\underline{W}}_{4c})\\ &+\frac{\partial \underline{\Phi}}{\partial \underline{B}_4}\Big|_{\underline{B}_4=\hat{\underline{B}}_4}(\underline{B}_4^*-\hat{\underline{B}}_4)+\frac{\partial \underline{\Phi}}{\partial \underline{W}_3}\Big|_{\underline{W}_3=\hat{\underline{W}}_3}(\underline{W}_3^*-\hat{\underline{W}}_3)\\ &+\frac{\partial \underline{\Phi}}{\partial \underline{C}_2}\Big|_{\underline{C}_2=\hat{\underline{C}}_2}(\underline{C}_2^*-\hat{\underline{C}}_2)+\frac{\partial \underline{\Phi}}{\partial \underline{B}_2}\Big|_{\underline{B}_2=\hat{\underline{B}}_2}(\underline{B}_2^*-\hat{\underline{B}}_2)+\underline{O}_h\\ &=\underline{\Phi}_{\underline{W}_4}\widetilde{\underline{W}}_4+\underline{\Phi}_{\underline{W}_{4c}}\widetilde{\underline{W}}_{4c}+\underline{\Phi}_{\underline{B}_4}\widetilde{\underline{B}}_4+\underline{\Phi}_{\underline{W}_3}\widetilde{\underline{W}}_3+\underline{\Phi}_{\underline{C}_2}\widetilde{\underline{C}}_2\\ &+\underline{\Phi}_{\underline{B}_2}\widetilde{\underline{B}}_2+\underline{O}_h\end{aligned} \tag{39}$$

$$\begin{aligned}\widetilde{\overline{\Phi}} &= \overline{\Phi}_{\overline{W}_4}\widetilde{\overline{W}}_4+\overline{\Phi}_{\overline{W}_{4c}}\widetilde{\overline{W}}_{4c}+\overline{\Phi}_{\overline{B}_4}\widetilde{\overline{B}}_4+\overline{\Phi}_{\overline{W}_3}\widetilde{\overline{W}}_3+\overline{\Phi}_{\overline{C}_2}\widetilde{\overline{C}}_2\\ &+\overline{\Phi}_{\overline{B}_2}\widetilde{\overline{B}}_2+\overline{O}_h\end{aligned} \tag{40}$$

where $\underline{O}_h$ and $\overline{O}_h$ are the vectors of higher order terms, and the above partial derivatives are consistent with the Jacobian matrix arrangement, and the result is:

$$\underline{\Phi}_{\underline{W}_4}=\left[\frac{\partial \underline{\phi}}{\partial \underline{\omega}^4}\right]_{1\times 1} \tag{41}$$

$$\underline{\Phi}_{\underline{W}_{4c}}=\left[\frac{\partial \underline{\phi}}{\partial \underline{\omega}^{4c}}\right]_{1\times 1} \tag{42}$$

$$\underline{\Phi}_{\underline{B}_4}=\left[\frac{\partial \underline{\phi}}{\partial \underline{b}^4}\right]_{1\times 1} \tag{43}$$

$$\underline{\Phi}_{\underline{W}_3}=\left[\frac{\partial \underline{\phi}}{\partial \underline{\omega}_1^3},\frac{\partial \underline{\phi}}{\partial \underline{\omega}_2^3},\cdots,\frac{\partial \underline{\phi}}{\partial \underline{\omega}_k^3}\right]_{1\times k} \tag{44}$$

$$\underline{\Phi}_{\underline{C}_2}=\left[\frac{\partial \underline{\phi}}{\partial \underline{c}_{11}^2},\cdots,\frac{\partial \underline{\phi}}{\partial \underline{c}_{1j}^2},\frac{\partial \underline{\phi}}{\partial \underline{c}_{21}^2},\cdots,\frac{\partial \underline{\phi}}{\partial \underline{c}_{ij}^2}\right]_{1\times(i\times j)} \tag{45}$$

$$\underline{\Phi}_{\underline{B}_2}=\left[\frac{\partial \underline{\phi}}{\partial \underline{b}_{11}^2},\cdots,\frac{\partial \underline{\phi}}{\partial \underline{b}_{1j}^2},\frac{\partial \underline{\phi}}{\partial \underline{b}_{21}^2},\cdots,\frac{\partial \underline{\phi}}{\partial \underline{b}_{ij}^2}\right]_{1\times(i\times j)} \tag{46}$$

$$\overline{\Phi}_{\overline{W}_4}=\left[\frac{\partial \overline{\phi}}{\partial \overline{\omega}^4}\right]_{1\times 1} \tag{47}$$

$$\overline{\Phi}_{\overline{W}_{4c}}=\left[\frac{\partial \overline{\phi}}{\partial \overline{\omega}^{4c}}\right]_{1\times 1} \tag{48}$$

$$\overline{\Phi}_{\overline{B}_4}=\left[\frac{\partial \overline{\phi}}{\partial \overline{b}^4}\right]_{1\times 1} \tag{49}$$

$$\overline{\Phi}_{\overline{W}_3}=\left[\frac{\partial \overline{\phi}}{\partial \overline{\omega}_1^3},\frac{\partial \overline{\phi}}{\partial \overline{\omega}_2^3},\cdots,\frac{\partial \overline{\phi}}{\partial \overline{\omega}_k^3}\right]_{1\times k} \tag{50}$$

$$\overline{\Phi}_{\overline{C}_2}=\left[\frac{\partial \overline{\phi}}{\partial \overline{c}_{11}^2},\cdots,\frac{\partial \overline{\phi}}{\partial \overline{c}_{1j}^2},\frac{\partial \overline{\phi}}{\partial \overline{c}_{21}^2},\cdots,\frac{\partial \overline{\phi}}{\partial \overline{c}_{ij}^2}\right]_{1\times(i\times j)} \tag{51}$$

$$\overline{\Phi}_{\overline{B}_2}=\left[\frac{\partial \overline{\phi}}{\partial \overline{b}_{11}^2},\cdots,\frac{\partial \overline{\phi}}{\partial \overline{b}_{1j}^2},\frac{\partial \overline{\phi}}{\partial \overline{b}_{21}^2},\cdots,\frac{\partial \overline{\phi}}{\partial \overline{b}_{ij}^2}\right]_{1\times(i\times j)} \tag{52}$$

By substituting (39) and (40) into (38), it can be obtained:

$$\begin{aligned}\widetilde{f} &= \underline{\hat{W}}_5{}^T\underline{\Phi}_{\underline{W}_4}\underline{\widetilde{W}}_4 + \underline{\hat{W}}_5{}^T\underline{\Phi}_{\underline{W}_{4c}}\underline{\widetilde{W}}_{4c} + \underline{\hat{W}}^T{}_5\underline{\Phi}_{\underline{B}_4}\underline{\widetilde{B}}_4 \\ &+\underline{\hat{W}}_5{}^T\underline{\Phi}_{\underline{W}_3}\underline{\widetilde{W}}_3 + \underline{\hat{W}}_5{}^T\underline{\Phi}_{\underline{C}_2}\underline{\widetilde{C}}_2 + \underline{\hat{W}}_5{}^T\underline{\Phi}_{\underline{B}_2}\underline{\widetilde{B}}_2 + \underline{\widetilde{W}}_5{}^T\underline{\hat{\Phi}} \\ &+\underline{\hat{W}}_5{}^T\overline{\Phi}_{\overline{W}_4}\overline{\widetilde{W}}_4 + \underline{\hat{W}}_5{}^T\overline{\Phi}_{\overline{W}_{4c}}\overline{\widetilde{W}}_{4c} + \underline{\hat{W}}_5{}^T\overline{\Phi}_{\overline{B}_4}\overline{\widetilde{B}}_4 + \underline{\hat{W}}_5{}^T\overline{\Phi}_{\overline{W}_3}\overline{\widetilde{W}}_3 \\ &+\underline{\hat{W}}_5{}^T\overline{\Phi}_{\overline{C}_2}\overline{\widetilde{C}}_2 + \underline{\hat{W}}_5{}^T\overline{\Phi}_{\overline{B}_2}\overline{\widetilde{B}}_2 + \underline{\widetilde{W}}_5{}^T\underline{\hat{\Phi}} + \Delta_0\end{aligned} \tag{53}$$

where the total higher order approximation error is:

$$\Delta_0 = \underline{\hat{W}}_5\underline{O}_h + \overline{\hat{W}}_5\overline{O}_h + \varepsilon_0 \tag{54}$$

Theorem 1. *Considering the system of APF in (8), the proposed IT2FNN-SFR STSMC strategy is guaranteed to be stable if the controller is designed as (33) and the parameter adaptive laws are designed properly as (55)–(69):*

$$\underline{\dot{\hat{W}}}_4{}^T = -\underline{\dot{\widetilde{W}}}_4{}^T = \eta_1 \mathrm{Csgn}(s)\underline{\hat{W}}_5{}^T\underline{\Phi}_{\underline{W}_4} \tag{55}$$

$$\overline{\dot{\hat{W}}}_4{}^T = -\overline{\dot{\widetilde{W}}}_4{}^T = \eta_2 \mathrm{Csgn}(s)\overline{\hat{W}}_5{}^T\overline{\Phi}_{\overline{W}_4} \tag{56}$$

$$\underline{\dot{\hat{W}}}_{4c}{}^T = -\underline{\dot{\widetilde{W}}}_{4c}{}^T = \eta_3 \mathrm{Csgn}(s)\underline{\hat{W}}_5{}^T\underline{\Phi}_{\underline{W}_{4c}} \tag{57}$$

$$\overline{\dot{\hat{W}}}_{4c}{}^T = -\overline{\dot{\widetilde{W}}}_{4c}{}^T = \eta_4 \mathrm{Csgn}(s)\overline{\hat{W}}_5{}^T\overline{\Phi}_{\overline{W}_{4c}} \tag{58}$$

$$\underline{\dot{\hat{B}}}_4{}^T = -\underline{\dot{\widetilde{B}}}_4{}^T = \eta_5 \mathrm{Csgn}(s)\overline{\hat{W}}_5{}^T\underline{\Phi}_{\underline{B}_4} \tag{59}$$

$$\overline{\dot{\hat{B}}}_4{}^T = -\overline{\dot{\widetilde{B}}}_4{}^T = \eta_6 \mathrm{Csgn}(s)\overline{\hat{W}}_5{}^T\underline{\Phi}_{\overline{B}_4} \tag{60}$$

$$\underline{\dot{\hat{W}}}_3{}^T = -\underline{\dot{\widetilde{W}}}_3{}^T = \eta_7 \mathrm{Csgn}(s)\underline{\hat{W}}_5{}^T\underline{\Phi}_{\underline{W}_3} \tag{61}$$

$$\overline{\dot{\hat{W}}}_3{}^T = -\overline{\dot{\widetilde{W}}}_3{}^T = \eta_8 \mathrm{Csgn}(s)\overline{\hat{W}}_5{}^T\overline{\Phi}_{\overline{W}_3} \tag{62}$$

$$\underline{\dot{\hat{C}}}_2{}^T = -\underline{\dot{\widetilde{C}}}_2{}^T = \eta_9 \mathrm{Csgn}(s)\underline{\hat{W}}_5{}^T\underline{\Phi}_{\underline{C}_2} \tag{63}$$

$$\overline{\dot{\hat{C}}}_2{}^T = -\overline{\dot{\widetilde{C}}}_2{}^T = \eta_{10} \mathrm{Csgn}(s)\overline{\hat{W}}_5{}^T\overline{\Phi}_{\overline{C}_2} \tag{64}$$

$$\underline{\dot{\hat{B}}}_2{}^T = -\underline{\dot{\widetilde{B}}}_2{}^T = \eta_{11} \mathrm{Csgn}(s)\overline{\hat{W}}_5{}^T\underline{\Phi}_{\underline{B}_2} \tag{65}$$

$$\overline{\dot{\hat{B}}}_2{}^T = -\overline{\dot{\widetilde{B}}}_2{}^T = \eta_{12} \mathrm{Csgn}(s)\overline{\hat{W}}_5{}^T\underline{\Phi}_{\overline{B}_2} \tag{66}$$

$$\underline{\dot{\hat{W}}}_5 = -\underline{\dot{\widetilde{W}}}_5 = \eta_{13} \mathrm{Csgn}(s)\underline{\hat{\Phi}} \tag{67}$$

$$\overline{\dot{\hat{W}}}_5 = -\overline{\dot{\widetilde{W}}}_5 = \eta_{14} \mathrm{Csgn}(s)\overline{\hat{\Phi}} \tag{68}$$

$$\dot{\hat{k}}_1 = -\dot{\tilde{k}}_1 = \eta_{15} C b |s|^{\frac{1}{2}} \tag{69}$$

where $\eta_1 \sim \eta_{15}$ *are the learning rates of the corresponding adaptive gains, which are positive constants.*

Proof. When $s \neq 0$, a Lyapunov function candidate is given as:

$$\begin{aligned} V &= |s| + \tfrac{1}{2\eta_1} tr\left(\underline{\widetilde{W}}_4{}^T \underline{\widetilde{W}}_4\right) + \tfrac{1}{2\eta_2} tr\left(\underline{\widetilde{\widetilde{W}}}_4{}^T \underline{\widetilde{\widetilde{W}}}_4\right) \\ &+ \tfrac{1}{2\eta_3} tr\left(\underline{\widetilde{W}}_{4c}{}^T \underline{\widetilde{W}}_{4c}\right) + \tfrac{1}{2\eta_4} tr\left(\underline{\widetilde{\widetilde{W}}}_{4c}{}^T \underline{\widetilde{\widetilde{W}}}_{4c}\right) \\ &+ \tfrac{1}{2\eta_5} tr\left(\underline{\widetilde{B}}_4{}^T \underline{\widetilde{B}}_4\right) + \tfrac{1}{2\eta_6} tr\left(\underline{\widetilde{\widetilde{B}}}_4{}^T \underline{\widetilde{\widetilde{B}}}_4\right) \\ &+ \tfrac{1}{2\eta_7} tr\left(\underline{\widetilde{W}}_3{}^T \underline{\widetilde{W}}_3\right) + \tfrac{1}{2\eta_8} tr\left(\underline{\widetilde{\widetilde{W}}}_3{}^T \underline{\widetilde{\widetilde{W}}}_3\right) \\ &+ \tfrac{1}{2\eta_9} tr\left(\underline{\widetilde{C}}_2{}^T \underline{\widetilde{C}}_2\right) + \tfrac{1}{2\eta_{10}} tr\left(\underline{\widetilde{\widetilde{C}}}_2{}^T \underline{\widetilde{\widetilde{C}}}_2\right) \\ &+ \tfrac{1}{2\eta_{11}} tr\left(\underline{\widetilde{B}}_2{}^T \underline{\widetilde{B}}_2\right) + \tfrac{1}{2\eta_{12}} tr\left(\underline{\widetilde{\widetilde{B}}}_2{}^T \underline{\widetilde{\widetilde{B}}}_2\right) \\ &+ \tfrac{1}{2\eta_{13}} tr\left(\underline{\widetilde{W}}_5{}^T \underline{\widetilde{W}}_5\right) + \tfrac{1}{2\eta_{14}} tr\left(\underline{\widetilde{\widetilde{W}}}_5{}^T \underline{\widetilde{\widetilde{W}}}_5\right) \\ &+ \tfrac{1}{2\eta_{15}} \tilde{k}_1{}^2 + \tfrac{Cbk_2}{2} \left(\int \mathrm{sgn}(s) dt\right)^2 \end{aligned} \tag{70}$$

The derivative of Equation (70) is obtained:

$$\begin{aligned} \dot{V} &= \mathrm{sgn}(s) \cdot \dot{s} + \tfrac{1}{\eta_1} \dot{\underline{\widetilde{W}}}_4{}^T \underline{\widetilde{W}}_4 + \tfrac{1}{\eta_2} \dot{\underline{\widetilde{\widetilde{W}}}}_4{}^T \underline{\widetilde{\widetilde{W}}}_4 + \tfrac{1}{\eta_3} \dot{\underline{\widetilde{W}}}_{4c}{}^T \underline{\widetilde{W}}_{4c} \\ &+ \tfrac{1}{\eta_4} \dot{\underline{\widetilde{\widetilde{W}}}}_{4c}{}^T \underline{\widetilde{\widetilde{W}}}_{4c} + \tfrac{1}{\eta_5} \dot{\underline{\widetilde{B}}}_4{}^T \underline{\widetilde{B}}_4 + \tfrac{1}{\eta_6} \dot{\underline{\widetilde{\widetilde{B}}}}_4{}^T \underline{\widetilde{\widetilde{B}}}_4 + \tfrac{1}{\eta_7} \dot{\underline{\widetilde{W}}}_3{}^T \underline{\widetilde{W}}_3 \\ &+ \tfrac{1}{\eta_8} \dot{\underline{\widetilde{\widetilde{W}}}}_3{}^T \underline{\widetilde{\widetilde{W}}}_3 + \tfrac{1}{\eta_9} \dot{\underline{\widetilde{C}}}_2{}^T \underline{\widetilde{C}}_2 + \tfrac{1}{\eta_{10}} \dot{\underline{\widetilde{\widetilde{C}}}}_2{}^T \underline{\widetilde{\widetilde{C}}}_2 + \tfrac{1}{\eta_{11}} \dot{\underline{\widetilde{B}}}_2{}^T \underline{\widetilde{B}}_2 \\ &+ \tfrac{1}{\eta_{12}} \dot{\underline{\widetilde{\widetilde{B}}}}_2{}^T \underline{\widetilde{\widetilde{B}}}_2 + \tfrac{1}{\eta_{13}} \underline{\widetilde{W}}_5{}^T \dot{\underline{\widetilde{W}}}_5 + \tfrac{1}{\eta_{14}} \underline{\widetilde{\widetilde{W}}}_5{}^T \dot{\underline{\widetilde{\widetilde{W}}}}_5 + \tfrac{1}{\eta_{15}} \tilde{k}_1 \cdot \dot{\tilde{k}}_1 \\ &+ Cbk_2 \mathrm{sgn}(s) \int \mathrm{sgn}(s) dt \end{aligned} \tag{71}$$

To simplify the proof process, define that:

$$\begin{aligned} \dot{H} &= \tfrac{1}{\eta_1} \dot{\underline{\widetilde{W}}}_4{}^T \underline{\widetilde{W}}_4 + \tfrac{1}{\eta_2} \dot{\underline{\widetilde{\widetilde{W}}}}_4{}^T \underline{\widetilde{\widetilde{W}}}_4 + \tfrac{1}{\eta_3} \dot{\underline{\widetilde{W}}}_{4c}{}^T \underline{\widetilde{W}}_{4c} + \tfrac{1}{\eta_4} \dot{\underline{\widetilde{\widetilde{W}}}}_{4c}{}^T \underline{\widetilde{\widetilde{W}}}_{4c} \\ &+ \tfrac{1}{\eta_5} \dot{\underline{\widetilde{B}}}_4{}^T \underline{\widetilde{B}}_4 + \tfrac{1}{\eta_6} \dot{\underline{\widetilde{\widetilde{B}}}}_4{}^T \underline{\widetilde{\widetilde{B}}}_4 + \tfrac{1}{\eta_7} \dot{\underline{\widetilde{W}}}_3{}^T \underline{\widetilde{W}}_3 + \tfrac{1}{\eta_8} \dot{\underline{\widetilde{\widetilde{W}}}}_3{}^T \underline{\widetilde{\widetilde{W}}}_3 \\ &+ \tfrac{1}{\eta_9} \dot{\underline{\widetilde{C}}}_2{}^T \underline{\widetilde{C}}_2 + \tfrac{1}{\eta_{10}} \dot{\underline{\widetilde{\widetilde{C}}}}_2{}^T \underline{\widetilde{\widetilde{C}}}_2 + \tfrac{1}{\eta_{11}} \dot{\underline{\widetilde{B}}}_2{}^T \underline{\widetilde{B}}_2 + \tfrac{1}{\eta_{12}} \dot{\underline{\widetilde{\widetilde{B}}}}_2{}^T \underline{\widetilde{\widetilde{B}}}_2 \\ &+ \tfrac{1}{\eta_{13}} \underline{\widetilde{W}}_5{}^T \dot{\underline{\widetilde{W}}}_5 + \tfrac{1}{\eta_{14}} \underline{\widetilde{\widetilde{W}}}_5{}^T \dot{\underline{\widetilde{\widetilde{W}}}}_5 + \tfrac{1}{\eta_{15}} \tilde{k}_1 \cdot \dot{\tilde{k}}_1 \end{aligned} \tag{72}$$

Substituting (30) and (72) into (71) obtains:

$$\begin{aligned} \dot{V} &= C\mathrm{sgn}(s) \cdot \left(f + bu - \dot{r}\right) + \dot{H} + Cbk_2 \mathrm{sgn}(s) \int \mathrm{sgn}(s) dt \\ &= Cs(f - \hat{f}) - Cb\hat{k}_1 |s|^{\frac{1}{2}} + \dot{H} \end{aligned} \tag{73}$$

If the conditions in Theorem 1 are satisfied, one can obtained:

$$\begin{aligned} \dot{V} &= C\mathrm{sgn}(s) \cdot \Delta_0 - Cb\hat{k}_1 |s|^{\frac{1}{2}} + \tfrac{1}{\eta_{15}} \tilde{k}_1 \cdot \dot{\tilde{k}}_1 \\ &= C\mathrm{sgn}(s) \cdot \Delta_0 - Cbk_1^* |s|^{\frac{1}{2}} \\ &\leq -Cbk_1^* |s|^{\frac{1}{2}} + C|\Delta_0| \end{aligned} \tag{74}$$

Suppose that the total higher order approximation error $|\Delta_0|$ has an upper bound, that is, $|\Delta_0| < \Delta_{\max}$. It can be obtained that:

$$\begin{cases} \dot{V} \leq 0 \ \ |s| \geq \left(\frac{\Delta_{\max}}{bk_1^*}\right)^2 \\ \dot{V} > 0 \ \ |s| < \left(\frac{\Delta_{\max}}{bk_1^*}\right)^2 \end{cases} \tag{75}$$

When the system is stable, it is clear that s will tend to 0, and when $\dot{V} > 0$, the changes of s is unknown. However, it can be concluded that s will eventually converge to:

$$-\left(\frac{\Delta_{\max}}{bk_1^*}\right)^2 \leq s \leq \left(\frac{\Delta_{\max}}{bk_1^*}\right)^2 \tag{76}$$

When it comes to $s = 0$, it is easy to find that it meets the requirement in Equation (76).

$$-\frac{1}{C}\left(\frac{\Delta_{\max}}{bk_1^*}\right)^2 \leq e \leq \frac{1}{C}\left(\frac{\Delta_{\max}}{bk_1^*}\right)^2 \tag{77}$$

As for e, it can be easily to conclude that e is bounded and the system is stable. □

Remark 1. *When the neural network performs parameter self-learning, matrix operations and partial derivative calculations are required, which will inevitably increase the amount of calculation. Table 1 gives the calculation time of the four control methods. Although the proposed method increases the computational complexity, the computational burden of the design method is relatively small while meeting the APF performance requirements. However, further optimization remains to be done.*

Table 1. The computational time of four control method.

Strategy	ASMC	FNNASMC-SFR based on LESO [41]	IT2FNN-SFR STSMC	CTSMC-MLNN [42]
Time(s)	5.5619	15.795	28.234	32.829

4. Numerical Verification

The effectiveness and reliability of the novel control strategy for APF system is verified on MATLAB/Simulink. The simulation experiment and comparative results are introduced below.

In the simulation process, the CPU is i5-8300H(2.30 GHz), the system is 64-bit and the version of MATLAB is 2019b.

A traditional PI controller is used in the DC voltage control of APF. The parameters of PI controller are given as: $K_P = 0.15$, $K_I = 0.02$. The designed controller in this paper is applied in the current control of APF system. The parameters of the membership function of IT2FNN in this article are selected by experts as follows:

$$\underline{C}_2 = \begin{bmatrix} 0.4 & 0.02 & -0.02 \\ 8 & 1 & -1 \end{bmatrix}; \ \underline{B}_2 = \begin{bmatrix} 1 & 1 & 1 \\ 5 & 5 & 5 \end{bmatrix}$$

$$\overline{C}_2 = \begin{bmatrix} 0.6 & 0.05 & -0.05 \\ 10 & 2 & -2 \end{bmatrix}; \ \overline{B}_2 = \begin{bmatrix} 1.2 & 1.2 & 1.2 \\ 3 & 3 & 3 \end{bmatrix}$$

In addition, the parameters of the STSMC and the related parameters of the adaptive law are selected as follows: $C = 10$, $k_2 = 2.5$, $\eta_1 = 2250$, $\eta_2 = 2250$, $\eta_3 = 50$, $\eta_4 = 50$, $\eta_5 = 375$, $\eta_6 = 375$, $\eta_7 = 75$, $\eta_8 = 75$, $\eta_9 = 15$, $\eta_{10} = 15$, $\eta_{11} = 40$, $\eta_{12} = 40$, $\eta_{13} = 20,000$, $\eta_{14} = 22,500$, $\eta_{15} = 0.0009$.

The other parameters used in the simulation process are shown in Table 2.

Table 2. Parameters for Simulation.

Parameters	Values
Supply voltage	24 V/50 Hz
APF main circuit	$L = 18$ mH, $R = 0.1$ Ω, $C_0 = 2200$ μF, $U_{dc} = 50$ V
Non-linear load at steady state	$R_1 = 5$ Ω, $R_2 = 15$ Ω, $C_1 = 1000$ uF
Additional non-linear load in parallel	$R_1 = 15$ Ω, $R_2 = 15$ Ω, $C_2 = 1000$ uF
Sampling time	$T_s = 1\ e^{-5}$s

When the APF does not work out, the power supply current is the same as the load current, which is shown in Figure 4. It is not difficult to find that the power supply current is severely polluted by distortion, and the THD of the power supply current is 40.30% (as shown in Figure 5). At 0 s, APF is integrated into the power grid for harmonic compensation. The power supply current is shown in Figure 6, and it recovers to a sine wave in a very short time. The THD of supply current, as shown in Figure 7, is only 2.37%, which greatly eliminates harmonics and significantly improves current quality. Figures 8 and 9 are the compensation current tracking curve and tracking error curve under the designed controller. In the Figure 8, the red line represents the reference current and the blue line represents the compensation current. It can be seen that the compensation current i_c can track the expected reference current i_r perfectly, the tracking error can approach to zero in a very short time, which further verifies that the designed method has a great ability of harmonic compensation.

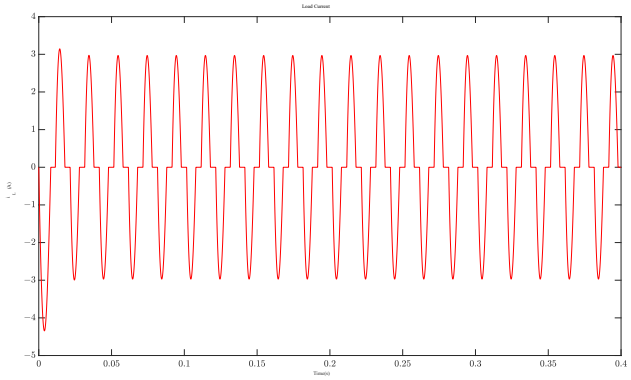

Figure 4. The power supply current before compensation.

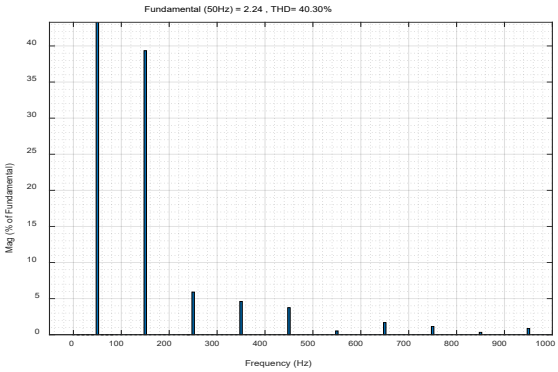

Figure 5. The spectrum analysis of power supply current before compensation.

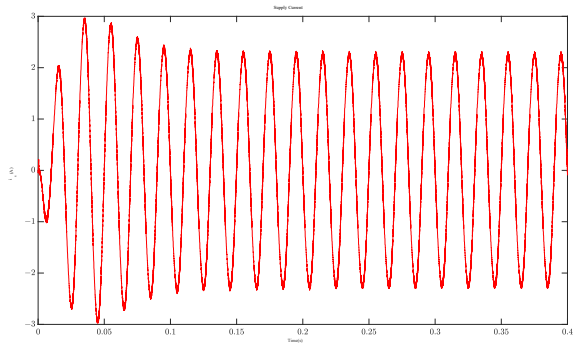

Figure 6. The power supply current after compensation.

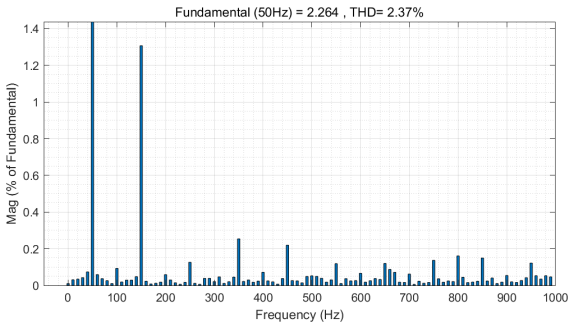

Figure 7. The spectrum analysis of power supply current after compensation.

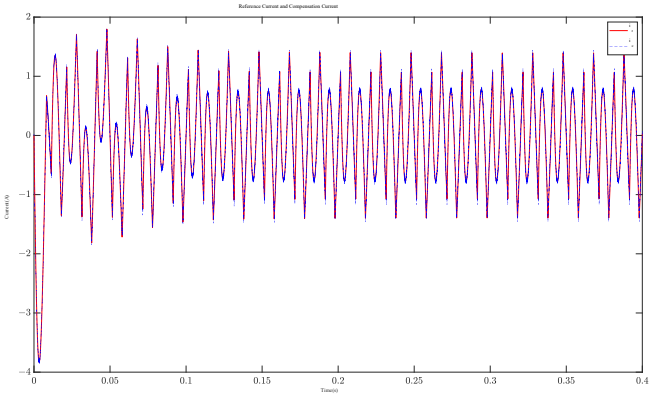

Figure 8. The compensation current tracking curve.

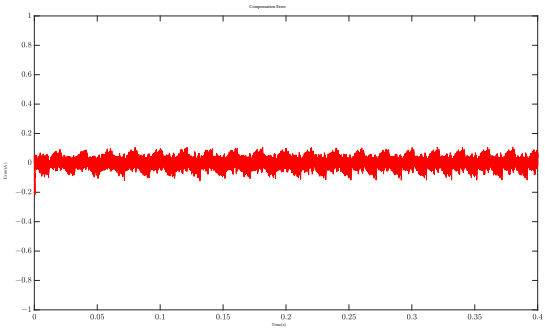

Figure 9. The compensation current tracking error curve.

At the same time, to verify the dynamic performance of the designed method, an additional nonlinear load was connected to the load at 0.5 s to make the total load of the circuit smaller, and the parallel load was disconnected at 0.7 s to make the total load of

the circuit larger. Figure 10 describes the power supply current curves of 0~0.9 s, 0.4~0.6 s, and 0.6~0.8 s from top to bottom, respectively. It can be seen from both the overall power supply current diagram and the amplification diagram of 0.1 s before and after the load change that the power supply current can maintain the sinusoidal waveform. According to Figures 11 and 12, the compensation current tracking curve and error curve still have good tracking performance when the load changes. The frequency spectrum analysis of the power supply current at 0.6 s and 0.8 s is shown in Figures 13 and 14. The THD is 1.64% after load connection and 2.58% after load disconnection, both of which have good performance.

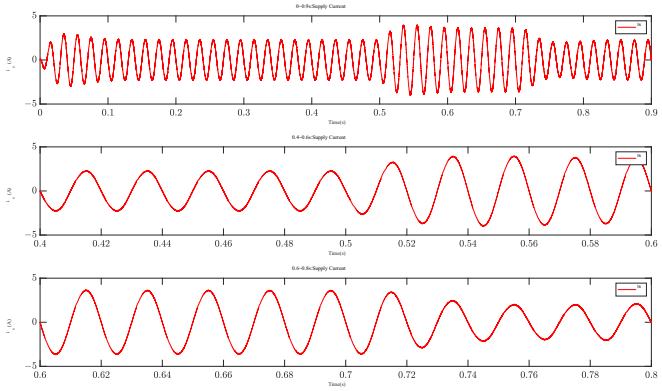

Figure 10. The power supply current of simulation experiment.

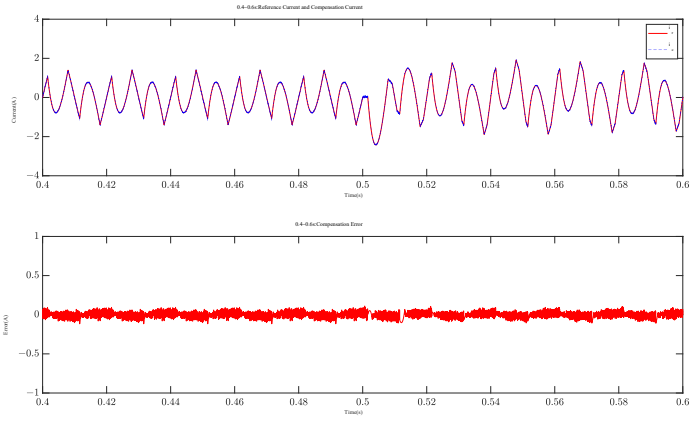

Figure 11. Current tracking and error curve when load is connected.

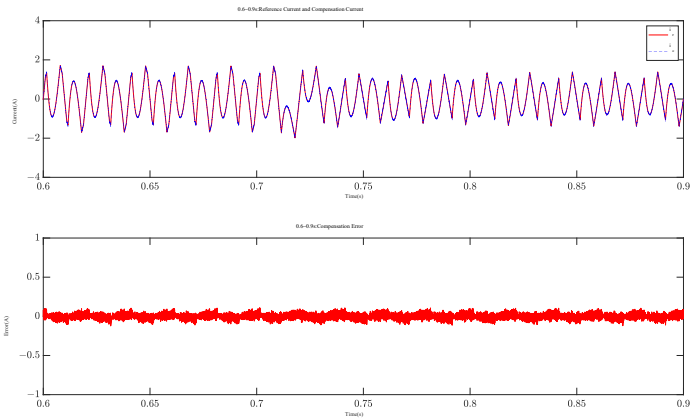

Figure 12. Current tracking and error curve when load is disconnected.

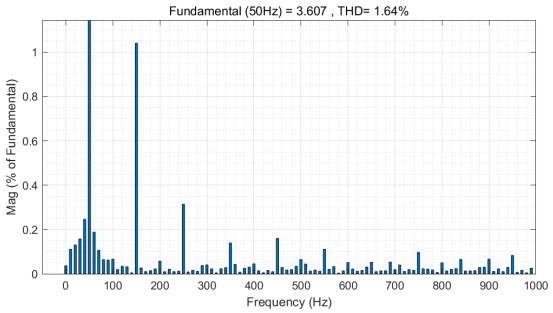

Figure 13. Power supply current spectrum analysis after load is connected.

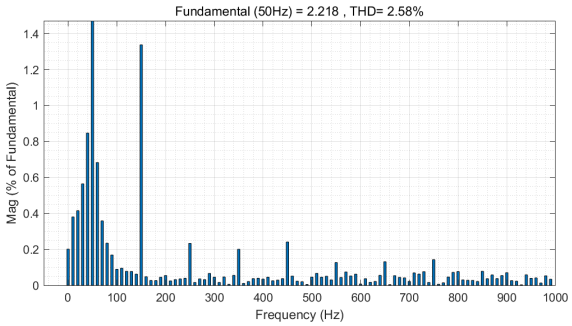

Figure 14. Power supply current spectrum analysis after load is disconnected.

In this paper, the output of the IT2FNN-SFR is taken as the practical mathematical model of APF, and the estimated curve is shown in Figure 15. The estimated curve has almost the same phase and similar amplitude compared with the ideal curve. Although there are many burrs and mutations, the estimated curve is more consistent with the actual situation for the system with actual parameter perturbation and external disturbance. Meanwhile, the adaptive gain of STSMC is shown in Figure 16, which estimates the stable value in a very short time, and its stable value is about 0.3.

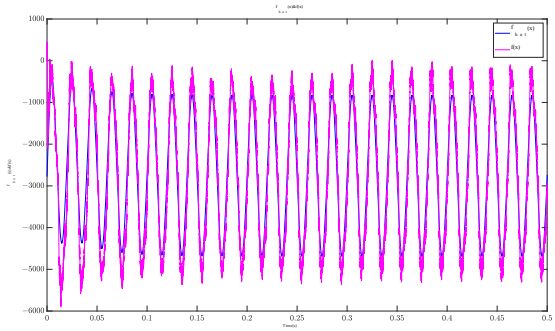

Figure 15. The output of the IT2FNN-SFR.

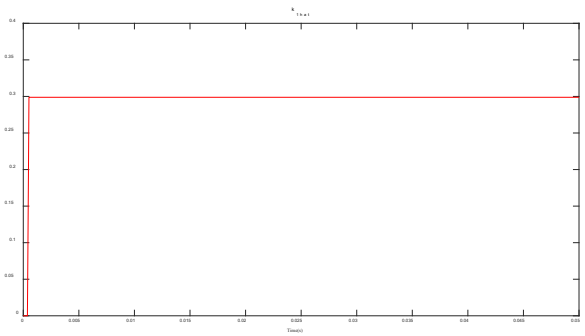

Figure 16. The gain of the adaptive STSMC.

At the same time, the adaptive curves of internal parameters in the designed neural network are depicted in Figure 17a–g. As shown in the figure, internal parameters will be adjusted adaptively and stabilized to the optimal value in a short time, which signifies that the NN has strong robustness and self-adaptive performance, and further verifies the superiority of the designed network.

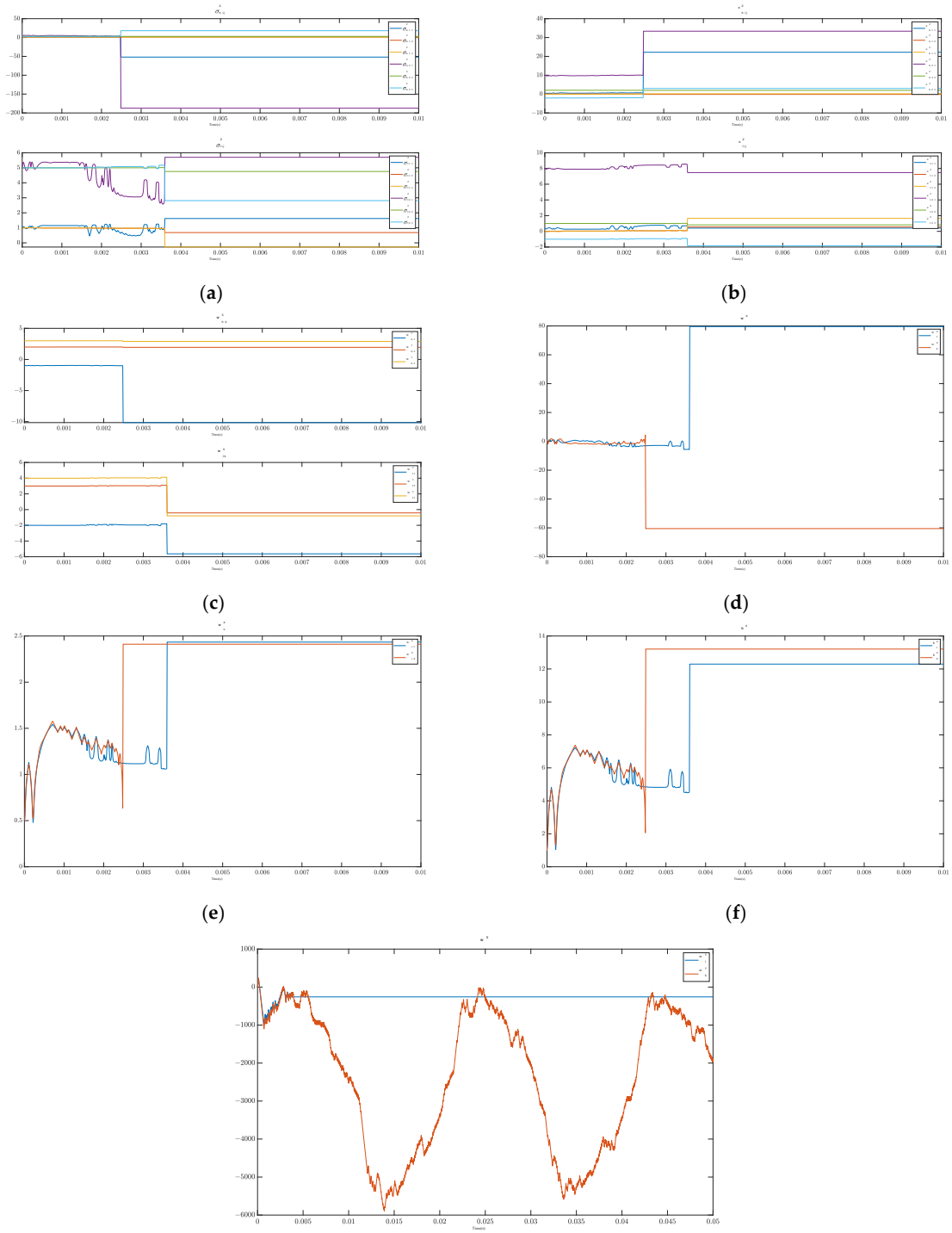

Figure 17. The adaptive curves of internal parameters in the IT2FNN-SFR. (**a**) The base width curves of membership function. (**b**) The center vector curves of membership function. (**c**) The input weight curves of SFR layer. (**d**) The weight curves of the SFR layer. (**e**) The self-feedback weight curves of SFR layer. (**f**) The bias term curves of SFR layer. (**g**) The output weight curves.

To verify that the proposed method in this paper can significantly weaken the inherent chattering in SMC, the control output comparison curve is given in Figure 18. Compared with the ASMC method (red curve), IT2FNN-SFR STSMC (blue curve) has a smaller control output amplitude range in a certain time period (take 0.2~0.3 s as an example). In addition, Table 3 gives the variance index of the control output, which can also verify the above conclusions.

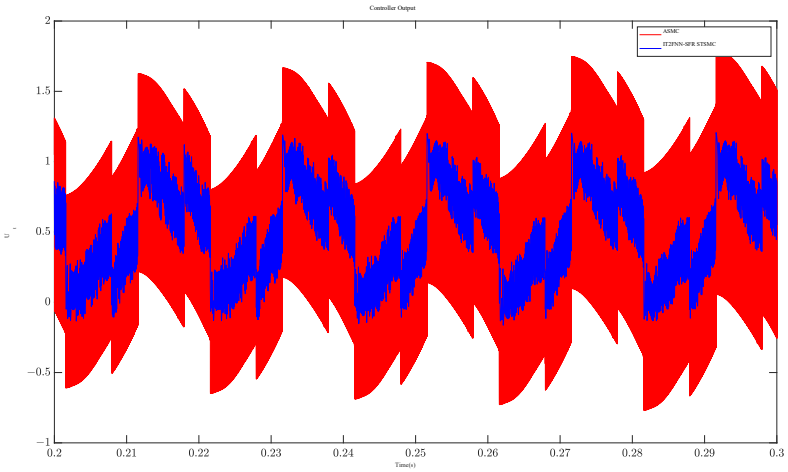

Figure 18. The control output comparison curve.

Table 3. The output variance of the two controllers.

Strategy Index	IT2FNN-SFR STSMC	ASMC
Output variance	0.0650	0.1362

Remark 2. *APF is a high-frequency switching power electronics, and its system output chattering is an important indicator to measure system performance. Variance is a statistic that measures the degree of dispersion of data, but large outliers may cause data skew, so the output is standardized as follows:*

$$u^*(t) = \frac{u(t) - u(t)_{\max}}{u(t)_{\max} - u(t)_{\min}} \tag{78}$$

The variance of the standardized control $u(t)^*$ *can be easily calculated, and the results are shown in Table 3.*

Meanwhile, the superiority of IT2FNN-SFR STSMC controller is illustrated by comparing with the adaptive sliding mode controller (ASMC). Figure 19 shows the error comparison curves of the two controllers. Compared with ASMC, the designed controller can track the desired signal more quickly and has a faster response speed at the initial moment. The overall tracking error is slightly less than that of ASMC controller, which indicates the compensation effect of the IT2FNN-SFR STSMC controller is better. The corresponding THD of the two controllers is also given in Table 4**.** It can be seen that the THD of the designed IT2FNN-SFR STSMC controller is slightly better than that of the ASMC controller in startup, steady state, and load changes.

Table 4. The corresponding THD of the two controllers.

Control Strategy	0 s	0.2 s	0.6 s	0.8 s
IT2FNN-SFR STSMC	16.44%	2.37%	1.64%	2.58%
ASMC	20.03%	2.66%	1.68%	2.92%

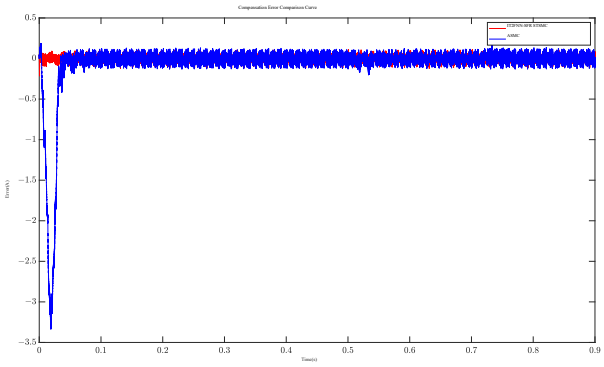

Figure 19. The compensation current error contrast curve.

5. Conclusions

In this paper, an adaptive super-twisting sliding mode control strategy for single-phase active power filter is proposed by combining interval type-2 fuzzy neural network with self-feedback recursion structure. The advantages of the IT2FNN and RNN are combined in the novel IT2FNN-SFR to obtain better dynamic approximation capacity. The new IT2FNN-SFR estimator is designed to approximate the unknown model of the system, improving the nonlinear processing ability and accuracy by using interval tpye-2 fuzzy membership function. At the same time, the self-feedback recursive structure can use the historical information to adjust the output, which improves the approximation ability of the network. The recursive structure in the NN will store the historical information to improve the accuracy of estimation and dynamic approximation character. The STSMC has cannot only effectively reduce system chattering, improve control accuracy, robustness, and system performance., but also simplify the parameter setting process. Finally, the simulation results show that the controller has good steady-state performance and dynamic response, and can effectively suppress the harmonics of the APF system.

Author Contributions: Conceptualization, J.F.; methodology, J.W.; writing—original draft preparation, J.W.; writing—review and editing, J.F. and Y.F. All authors have read and agreed to the published version of the manuscript.

Funding: This work is partially supported by National Science Foundation of China under Grant No. 62273131.

Data Availability Statement: All relevant data are within the manuscript.

Conflicts of Interest: The authors declare no conflict of interest.

References

1. Wu, Z.; Yang, Z.; Ding, K.; He, G. Order-Domain-Based Harmonic Injection Method for Multiple Speed Harmonics Suppression of PMSM. *IEEE Trans. Power Electron.* **2021**, *36*, 4478–4487. [CrossRef]
2. RGregory, R.; Azevedo, C.; Santos, I. Study of Harmonic Distortion Propagation from a Wind Park. *IEEE Lat. Am. Trans.* **2020**, *18*, 1077–1084. [CrossRef]
3. Jiao, N.; Wang, S.; Ma, J.; Chen, X.; Liu, T.; Zhou, D.; Yang, Y. The Closed-Loop Sideband Harmonic Suppression for CHB Inverter with Unbalanced Operation. *IEEE Trans. Power Electron.* **2022**, *37*, 5333–5341. [CrossRef]
4. Fu, J.; Chen, L.; Zhao, H.; Zhang, P. High and Low Frequency Control Strategy for APF DC Side Ripple Voltage under Unbalanced Load. In Proceedings of the 2019 IEEE 2nd International Conference on Electronics and Communication Engineering (ICECE), Xi'an, China, 9–11 December 2019; pp. 326–330.
5. Vahedi, H.; Shojaei, A.A.; Dessaint, L.-A.; Al-Haddad, K. Reduced DC-Link Voltage Active Power Filter Using Modified PUC5 Converter. *IEEE Trans. Power Electron.* **2018**, *33*, 943–947. [CrossRef]
6. Incremona, G.P.; Rubagotti, M.; Ferrara, A. Sliding Mode Control of Constrained Nonlinear Systems. *IEEE Trans. Autom. Control* **2017**, *62*, 2965–2972. [CrossRef]
7. Hou, L.; Ma, J.; Wang, W. Sliding Mode Predictive Current Control of Permanent Magnet Synchronous Motor with Cascaded Variable Rate Sliding Mode Speed Controller. *IEEE Access* **2022**, *10*, 33992–34002. [CrossRef]
8. Qu, L.; Qiao, W.; Qu, L. An Extended-State-Observer-Based Sliding-Mode Speed Control for Permanent-Magnet Synchronous Motors. *IEEE J. Emerg. Sel. Top. Power Electron.* **2021**, *9*, 1605–1613. [CrossRef]

9. Chen, X.; Li, Y.; Ma, H.; Tang, H.; Xie, Y. A Novel Variable Exponential Discrete Time Sliding Mode Reaching Law. *IEEE Trans. Circuits Syst. II Express Briefs* **2021**, *68*, 2518–2522. [CrossRef]
10. Liu, H.; Wang, H.; Sun, J. Attitude control for QTR using exponential nonsingular terminal sliding mode control. *J. Syst. Eng. Electron.* **2019**, *30*, 191–200.
11. Ren, L.; Lin, G.; Zhao, Y.; Liao, Z.; Peng, F. Adaptive Nonsingular Finite-Time Terminal Sliding Mode Control for Synchronous Reluctance Motor. *IEEE Access* **2021**, *9*, 51283–51293. [CrossRef]
12. Fei, J.; Wang, H.; Fang, Y. Novel Neural Network Fractional-Order Sliding-Mode Control with Application to Active Power Filter. *IEEE Trans. Syst. Man Cybern. Syst.* **2022**, *52*, 3508–3518. [CrossRef]
13. Bo, L.; Peng, J.; Chong, K.T.; Rodriguez, J.; Guerrero, J.M. Robust Fuzzy-Fractional-Order Nonsingular Terminal Sliding-Mode Control of LCL-Type Grid-Connected Converters. *IEEE Trans. Ind. Electron.* **2022**, *69*, 5854–5866.
14. Liu, Y.-J.; Chen, H. Adaptive Sliding Mode Control for Uncertain Active Suspension Systems with Prescribed Performance. *IEEE Trans. Syst. Man Cybern. Syst.* **2021**, *51*, 6414–6422. [CrossRef]
15. Roy, S.; Roy, S.B.; Lee, J.; Baldi, S. Overcoming the Underestimation and Overestimation Problems in Adaptive Sliding Mode Control. *IEEE/ASME Trans. Mechatron.* **2019**, *24*, 2031–2039. [CrossRef]
16. Roy, S.; Baldi, S.; Fridman, L.M. On adaptive sliding mode control without a priori bounded uncertainty. *Automatica* **2020**, *111*, 108650. [CrossRef]
17. Levant, A. Higher-order sliding modes, differentiation and output-feedback control. *Int. J. Control.* **2003**, *76*, 924–941. [CrossRef]
18. Guo, J. The Load Frequency Control by Adaptive High Order Sliding Mode Control Strategy. *IEEE Access* **2022**, *10*, 25392–25399. [CrossRef]
19. Shah, I.; Rehman, F.U. Smooth Second Order Sliding Mode Control of a Class of Underactuated Mechanical Systems. *IEEE Access* **2018**, *6*, 7759–7771. [CrossRef]
20. Chalanga, A.; Kamal, S.; Fridman, L.M.; Bandyopadhyay, B.; Moreno, J.A. Implementation of Super-Twisting Control: Super-Twisting and Higher Order Sliding-Mode Observer-Based Approaches. *IEEE Trans. Ind. Electron.* **2016**, *63*, 3677–3685. [CrossRef]
21. Wu, Y.; Ma, F.; Liu, X.; Hua, Y.; Liu, X.; Li, G. Super Twisting Disturbance Observer-Based Fixed-Time Sliding Mode Backstepping Control for Air-Breathing Hypersonic Vehicle. *IEEE Access* **2021**, *8*, 17567–17583. [CrossRef]
22. Wang, W.; Ma, J.; Li, X.; Cheng, Z.; Zhu, H.; Teo, C.S.; Lee, T.H. Iterative Super-Twisting Sliding Mode Control for Tray Indexing System with Unknown Dynamics. *IEEE Trans. Ind. Electron.* **2020**, *68*, 9855–9865. [CrossRef]
23. Merayo, N.; Juárez, D.; Aguado, J.C.; de Miguel, I.; Durán, R.J.; Fernández, P.; Lorenzo, R.M.; Abril, E.J. PID Controller Based on a Self-Adaptive Neural Network to Ensure QoS Bandwidth Requirements in Passive Optical Networks. *J. Opt. Commun. Netw.* **2017**, *9*, 433–445. [CrossRef]
24. Dai, W.; Zhang, L.; Fu, J.; Chai, T.; Ma, X. Dual-Rate Adaptive Optimal Tracking Control for Dense Medium Separation Process Using Neural Networks. *IEEE Trans. Neural Netw. Learn. Syst.* **2021**, *32*, 4202–4216. [CrossRef]
25. Yang, Y.; Ye, Y. Backstepping sliding mode control for uncertain strict-feedback nonlinear systems using neural-network-based adaptive gain scheduling. *J. Syst. Eng. Electron.* **2018**, *29*, 580–586.
26. Li, K.; Li, Y. Adaptive Neural Network Finite-Time Dynamic Surface Control for Nonlinear Systems. *IEEE Trans. Neural Netw. Learn. Syst.* **2021**, *32*, 5688–5697. [CrossRef]
27. Liu, X.; Su, C.-Y.; Yang, F. FNN Approximation-Based Active Dynamic Surface Control for Suppressing Chatter in Micro-Milling with Piezo-Actuators. *IEEE Trans. Syst. Man Cybern. Syst.* **2017**, *47*, 2100–2113. [CrossRef]
28. Wai, R.; Yao, J.; Lee, J. Backstepping Fuzzy-Neural-Network Control Design for Hybrid Maglev Transportation System. *IEEE Trans. Neural Netw. Learn. Syst.* **2015**, *26*, 302–317. [PubMed]
29. Wai, R.-J.; Chen, M.-W.; Liu, Y.-K. Design of Adaptive Control and Fuzzy Neural Network Control for Single-Stage Boost Inverter. *IEEE Trans. Ind. Electron.* **2015**, *62*, 5434–5445. [CrossRef]
30. Liu, L.; Fei, J. Extended State Observer Based Interval Type-2 Fuzzy Neural Network Sliding Mode Control with Its Application in Active Power Filter. *IEEE Trans. Power Electron.* **2022**, *37*, 5138–5154. [CrossRef]
31. Wang, J.; Luo, W.; Liu, J.; Wu, L. Adaptive Type-2 FNN-Based Dynamic Sliding Mode Control of DC–DC Boost Converters. *IEEE Trans. Syst. Man, Cybern. Syst.* **2021**, *51*, 2246–2257. [CrossRef]
32. Gao, Y.; Liu, J.; Wang, Z.; Wu, L. Interval Type-2 FNN-Based Quantized Tracking Control for Hypersonic Flight Vehicles with Prescribed Performance. *IEEE Trans. Syst. Man Cybern. Syst.* **2021**, *51*, 1981–1993. [CrossRef]
33. Kim, C.-J.; Chwa, D. Obstacle Avoidance Method for Wheeled Mobile Robots Using Interval Type-2 Fuzzy Neural Network. *IEEE Trans. Fuzzy Syst.* **2015**, *23*, 677–687. [CrossRef]
34. Wai, R.-J.; Lin, C.-M.; Peng, Y.-F. Adaptive Hybrid Control for Linear Piezoelectric Ceramic Motor Drive Using Diagonal Recurrent CMAC Network. *IEEE Trans. Neural Netw.* **2004**, *15*, 1491–1506. [CrossRef] [PubMed]
35. Yogi, S.C.; Tripathi, V.K.; Behera, L. Adaptive Integral Sliding Mode Control Using Fully Connected Recurrent Neural Network for Position and Attitude Control of Quadrotor. *IEEE Trans. Neural Netw. Learn. Syst.* **2021**, *32*, 5595–5609. [CrossRef]
36. Fei, J.; Chen, Y.; Liu, L.; Fang, Y. Fuzzy Multiple Hidden Layer Recurrent Neural Control of Nonlinear System Using Terminal Sliding-Mode Controller. *IEEE Trans. Cybern.* **2022**, *52*, 9519–9534. [CrossRef]
37. Fei, J.; Liu, L. Real-Time Nonlinear Model Predictive Control of Active Power Filter Using Self-Feedback Recurrent Fuzzy Neural Network Estimator. *IEEE Trans. Ind. Electron.* **2022**, *69*, 8366–8376. [CrossRef]

38. Han, H.-G.; Zhang, L.; Hou, Y.; Qiao, J.-F. Nonlinear Model Predictive Control Based on a Self-Organizing Recurrent Neural Network. *IEEE Trans. Neural Networks Learn. Syst.* **2016**, *27*, 402–415. [CrossRef]
39. Fei, J.; Wang, Z.; Pan, Q. Self-Constructing Fuzzy Neural Fractional-Order Sliding Mode Control of Active Power Filter. *IEEE Trans. Neural Networks Learn. Syst.* **2022**. [CrossRef]
40. Fei, J.; Wang, Z.; Fang, Y. Self-Evolving Chebyshev Fuzzy Neural Fractional-Order Sliding Mode Control for Active Power Filter. *IEEE Trans. Ind. Inform.* **2022**, *19*, 2729–2739. [CrossRef]
41. Wang, J.; Fei, J. Self-Feedback Neural Network Sliding Mode Control with Extended State Observer for Active Power Filter. *IEEE Internet Things J.* **2023**. [CrossRef]
42. Zhang, L.; Fei, J. Intelligent Complementary Terminal Sliding Mode Using Multi-Loop Neural Network for Active Power Filter. *IEEE Trans. Power Electron.* **2023**. [CrossRef]